T cell activation requires force generation

Kenneth H. Hu[1] and Manish J. Butte[1,2]

[1]Stanford Biophysics and [2]Department of Pediatrics, Division of Allergy, Immunology, and Rheumatology, Stanford University, Stanford, CA 94305

Triggering of the T cell receptor (TCR) integrates both binding kinetics and mechanical forces. To understand the contribution of the T cell cytoskeleton to these forces, we triggered T cells using a novel application of atomic force microscopy (AFM). We presented antigenic stimulation using the AFM cantilever while simultaneously imaging with optical microscopy and measuring forces on the cantilever. T cells respond forcefully to antigen after calcium flux. All forces and calcium responses were abrogated upon treatment with an F-actin inhibitor. When we emulated the forces of the T cell using the AFM cantilever, even these actin-inhibited T cells became activated. Purely mechanical stimulation was not sufficient; the exogenous forces had to couple through the TCR. These studies suggest a mechanical–chemical feedback loop in which TCR-triggered T cells generate forceful contacts with antigen-presenting cells to improve access to antigen.

Introduction

Here, we study the mechanical forces generated by T cells undergoing activation. T cell receptors (TCRs) are triggered upon interaction with their cognate peptides presented in the major histocompatibility complex (pMHC). Recent work has suggested that triggering requires a force upon the TCR through shearing (Li et al., 2010) or pulling (Liu et al., 2014). The origin of these forces is as yet unknown, but the fact that TCR triggering occurs while T cells interact with inert objects such as antibody-coated beads suggests that the major contribution of force on the TCR comes from the T cell itself. Thermal forces can alter membrane shape to induce transient, solitary receptor–ligand contacts (Lee et al., 2003), whose binding energy can lead to further membrane apposition and further TCR triggering (James and Vale, 2012). The TCR could also be exposed to shear forces when T cells and APCs move relative to one another while interacting (Beemiller and Krummel, 2010).

After initial triggering, T cells can enhance contact with antigen-presenting cells (APCs) by actively pushing actin-rich lamellipodia and invadopodia into APCs (Negulescu et al., 1996; Sage et al., 2012). T cells plunge their invadopodia more than 1 µm deep into APCs (Ueda et al., 2011). Oscillatory movements of the actin cytoskeleton in the lamellipodium were observed for T cells interacting with pMHC on planar lipid bilayers and showed speeds of ∼0.04 µm/s for the cytoskeletal extensions, with a periodicity of ∼2 min (Sims et al., 2007). High-speed light-sheet imaging showed that T cells frenetically propel actin around the leading edge and periphery of synapses for ∼1 min after contact (Ritter et al., 2015). This prior work supports the importance of actin dynamics in enhancing T cell–APC contacts.

Atomic force microscopy (AFM) has been used to characterize the adhesive force between T cells and APCs and the force needed to uncouple individual TCR–pMHC bonds (Hosseini et al., 2009; Ma and Finkel, 2010; Puech et al., 2011) but has not been used to deliver antigenic signals to living cells except in our prior work with mast cells (Hu et al., 2014). Here, AFM allowed us to spatiotemporally control the delivery of TCR ligands while simultaneously measuring the T cell's biochemical and mechanical responses.

Results and discussion

We coated the AFM cantilever tip with molecules to stimulate T cells (anti-CD3 or pMHC; Fig. 1 A). To ensure stable attachment of proteins to the cantilever tip, we used the chemical crosslinker sulfosuccinimidyl 6-(3′-(2-pyridyldithio)propionamido) hexanoate (sulfo-LC-SPDP) to covalently attach streptavidin to a 3-mercaptopropyl trimethoxysilane–coated silicon cantilever (Fig. S1). Fluorescence imaging of phycoerythrin-labeled streptavidin showed that the tip was well coated (Fig. 1 B). Either biotinylated pMHC or biotinylated anti-CD3 was then added to the streptavidin-coated cantilever tip. We used a newly functionalized cantilever to interrogate each cell.

Primary effector $CD4^+$ T cells were obtained from TCR-transgenic OT-II mice, which recognize the ovalbumin peptide (323–339) in the context of $I\text{-}A^b$. We measured Ca^{2+} influx as a proximal readout for TCR triggering, measured by change in fluorescence intensity of the Ca^{2+}-sensitive dye Fluo-4. By gently touching the T cell surface with the anti-CD3–coated cantilever with a trigger force of 250 pN, we ligated TCR–CD3 complexes and monitored Fluo-4 intensity changes

Correspondence to Manish J. Butte: manish.butte@stanford.edu

Abbreviations used in this paper: AFM, atomic force microscope or microscopy; APC, antigen-presenting cell; CRAC, calcium release–activated channel; MLCK, myosin light chain kinase; pMHC, peptide bound to the major histocompatibility complex; sulfo-LC-SPDP, sulfosuccinimidyl 6-(3′-(2-pyridyldithio)propionamido) hexanoate; TCR, T cell receptor.

The Rockefeller University Press $30.00
J. Cell Biol. Vol. 213 No. 5 535–542
www.jcb.org/cgi/doi/10.1083/jcb.201511053

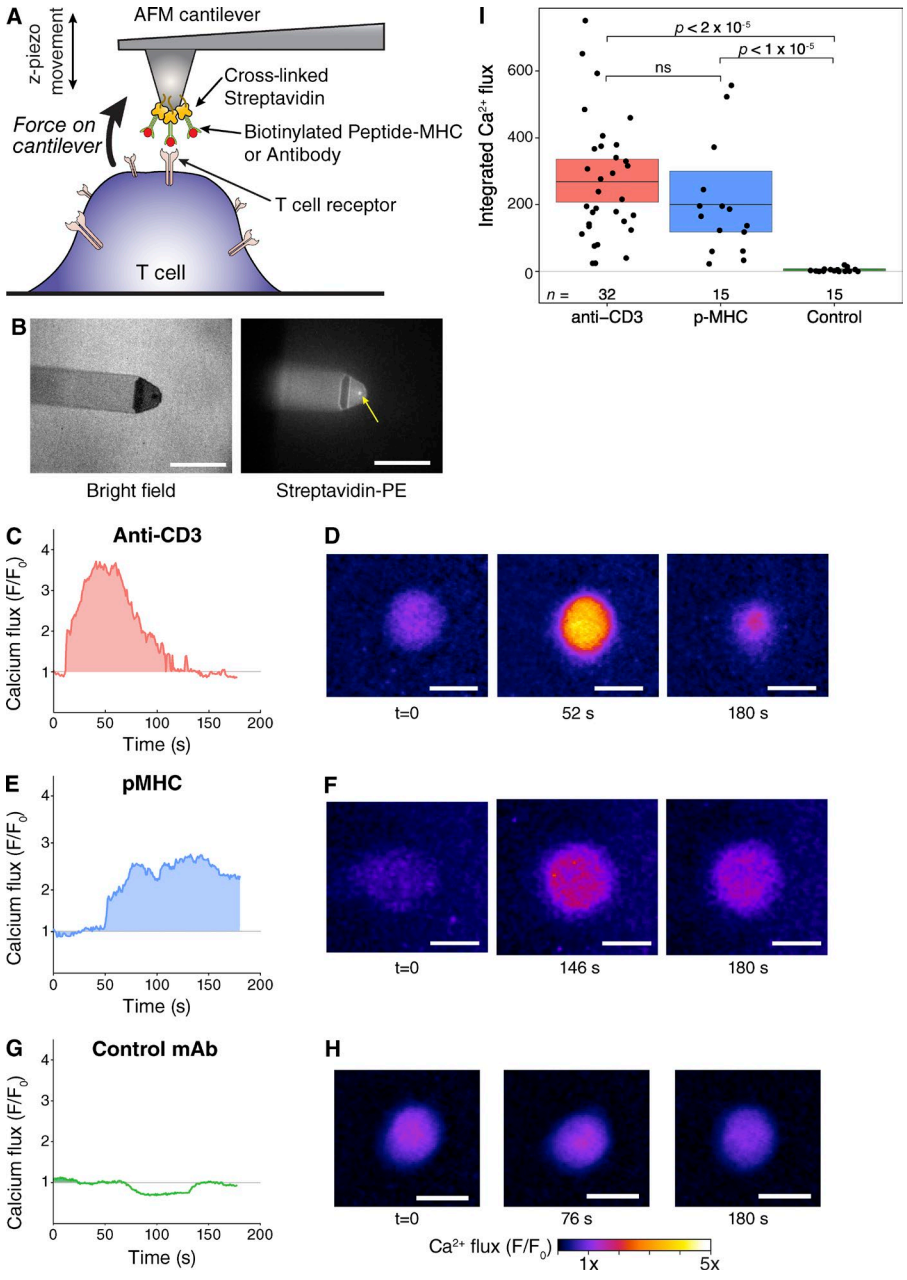

Figure 1. **AFM delivery of antigenic stimulation.** (A) Schematic showing AFM cantilever for stimulation of T cells and for monitoring mechanical responses. (B, left) Bright-field image of cantilever showing the dark silicon pad with the tip and the silicon nitride body of the cantilever. (right) Fluorescence image of fluorescent phycoerythrin-conjugated streptavidin assembled from a projection of multiple slices of spinning-disk confocal images. The cantilever tip is bright with labeled streptavidin (arrow). Bars, 50 µm. (C–I) Ca^{2+} responses to AFM-delivered stimulation. The AFM cantilever was brought into continuous contact with Fluo-4–labeled T cells for 180 s and imaged every 1 s. $t = 0$ is when the AFM force trigger was reached upon initial contact. Fluo-4 intensity was normalized to the Fluo-4 intensity at $t = 0$. Fluo-4 intensity in T cells contacted with a cantilever coated with anti-CD3 (C), pMHC (D), or irrelevant monoclonal antibody (hCD25 mAb; E). Shaded area under each curve represents the time-integrated calcium flux. (F–H) Fluorescent micrographs of the cells in C–E being touched at the start, peak flux, and end of experiment at the times shown. The cells are false colored according to the bar underneath. Bars, 5 µm. (I) Time-integrated Ca^{2+} flux shown for cantilevers coated with anti-CD3, pMHC, and control mAb. Data were pooled for pMHC ($n = 15$ across three independent experiments), anti-CD3 ($n = 32$ across nine independent experiments), and control antibody ($n = 15$ across four independent experiments). Each dot is a contact on one T cell. Box shows the bootstrapped mean and 95% CI. ns, not significant.

by fluorescence microscopy. With the cantilever in continuous contact, we observed pronounced Ca^{2+} flux (Fig. 1, C, D, and I). We also engaged T cells with cognate pMHC-coated cantilevers and observed a similar Ca^{2+} flux time profile and integrated intensity (Fig. 1, E, F, and I). In contrast, continuous contact with cantilevers coated with irrelevant monoclonal antibodies produced no significant Ca^{2+} flux (Fig. 1, G–I). For control mAbs in this work, we used both anti-CD43 and anti-CD25, which bound to cell-surface receptors (seen upon disengagement of the cantilever from the cell; not depicted) but would not be expected to activate T cells (Bunnell et al., 2002; Hosseini et al., 2009). To ensure that the increase in Fluo-4 intensity observed was truly indicative of Ca^{2+} entry and not shape changes in the T cell or changes in the focal plane upon contact with the AFM cantilever, we loaded the T cells with both Fluo-4 and Fura-Red dyes. We calculated the ratio of Fluo-4 to Fura-Red intensities and observed a similar time profile, indicating antigen-dependent Ca^{2+} flux (Fig. S2, A and B). These results indicate that AFM can deliver antigenic stimulation to T cells.

By monitoring the deflection of the AFM cantilever during contact with these same cells, we measured forces generated during activation. During continuous TCR triggering, the T cells exhibited large pushing and pulling forces on the cantilever (Fig. 2 A). In contrast, cells contacted with control mAb–coated cantilevers yielded no significant force generation (Fig. 2 B). We found that both pushing forces (Fig. 2 C) and pulling forces (Fig. 2 D) were higher in cells contacted with anti-CD3 than with control mAb. This result indicates that continuous TCR triggering results in the generation of forces by the T cell.

T cells pushed against pMHC-coated cantilevers comparably to anti-CD3–coated cantilevers (Fig. 2 C). However, we found weaker pulling forces (~2-fold less) on pMHC-coated cantilevers compared with anti-CD3–coated cantilevers (Fig. 2 D). We suspect this weaker pulling force was caused by the breaking

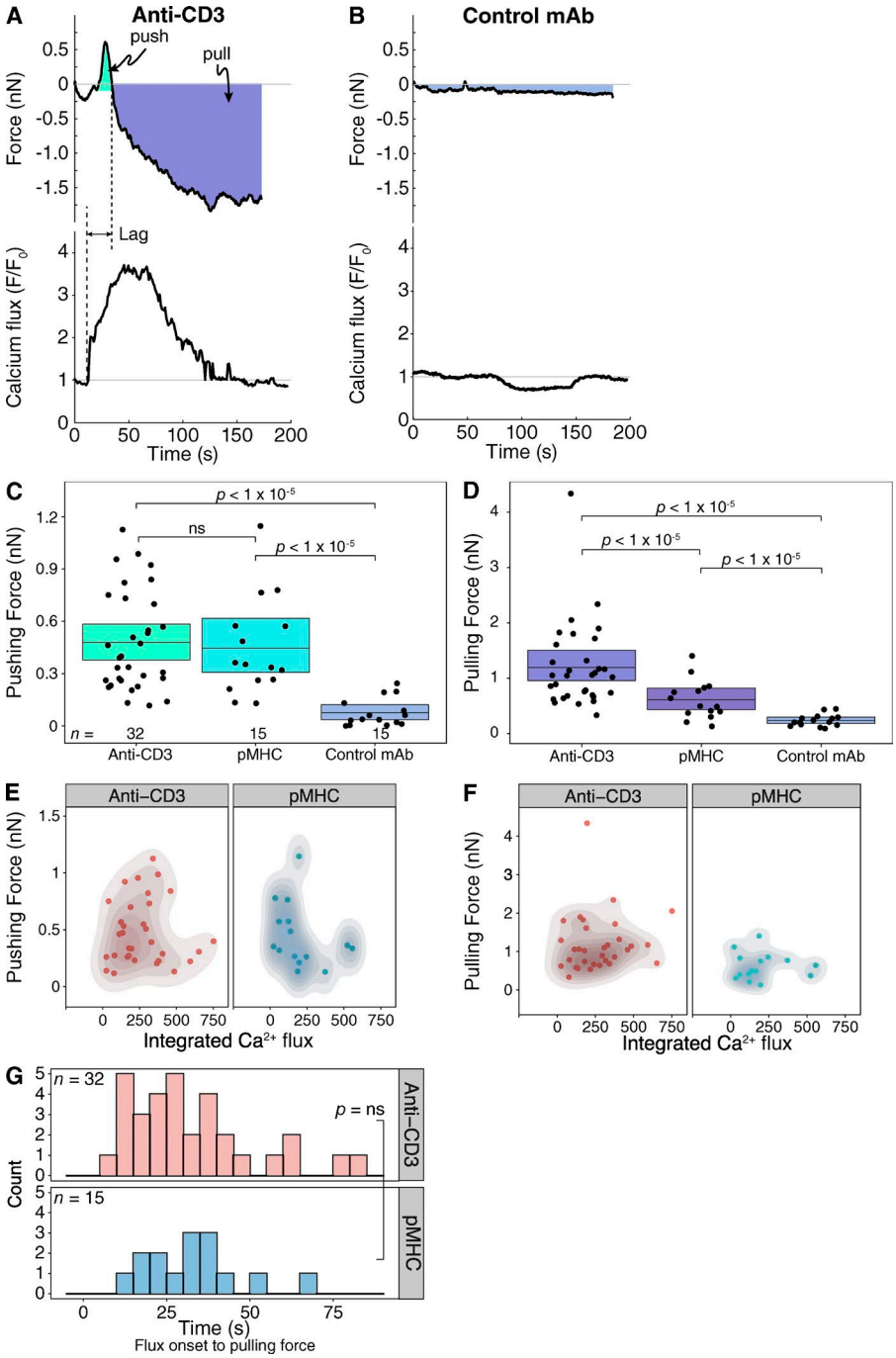

Figure 2. **Mechanical forces generated by AFM-delivered stimulation.** Time course of force exerted on the cantilever during contact with the T cell. Graphs begin with the trigger point at $t = 0$. The 0-force baseline is set to the deflection at the trigger point. All cells are the same as in Fig. 1. Cantilever was coated with anti-CD3 (A) or irrelevant mAb (B). The lightly shaded area represents the push phase. The magnitude of the push force is the height of the peak from the base, calculated from the inflection. The darker shaded region represents the pull phase, with the magnitude of the pull calculated from the minimum of the region to the 0-force baseline. The time lags in G are calculated as shown by the dashed lines. Magnitudes of pushing (C) forces and pulling (D) forces for cells stimulated with anti-CD3–coated cantilevers versus control antibody–coated cantilevers. These data are from the same cells used in Fig. 1. Boxes show the bootstrapped mean and 95% CI. ns, not significant. Time-integrated calcium flux versus magnitude of pushing (E) and pulling (F) forces. Density contours are shown in gray. (G) Histograms show the time lag between the onset of calcium flux to the start of the pulling force for anti-CD3–coated and pMHC-coated cantilevers.

of some noncovalent bonds in the relatively weaker interaction of pMHC with TCR compared with the interaction of anti-CD3 with CD3. Indeed, force spectroscopy and biophysical probe experiments have shown prompt unbinding of individual pMHC–TCR interactions under low pulling forces (Puech et al., 2011; Liu et al., 2014).

We found no correlation between the integrated Ca^{2+} flux and the magnitudes of either the pushing (Fig. 2 E) or pulling (Fig. 2 F) forces. The pushing force by T cells always preceded pulling, resulting in a consistent force–time profile (Fig. 2 A). To identify the temporal correlation between Ca^{2+} flux and pulling forces, we calculated the time lag between the onset of Ca^{2+} rise and the onset of pulling forces (Fig. 2, A and G). The mean (± 95% confidence interval [CI]) of this time lag was 32.5 ± 8.7 s for pMHC and 32.1 ± 7.2 s for anti-CD3. These results show that Ca^{2+} flux and force generation upon triggering are temporally correlated.

We next sought to dissect the molecular mechanisms of this force generation. Actin-rich structures spearhead contact with APCs, as mentioned earlier. Rapid accumulation of F-actin at the immune synapse is a hallmark of T cell activation (Billadeau et al., 2007) and serves important roles in T cell activation (Malissen and Bongrand, 2015). To determine whether actin polymerization was the source of the generated force, we treated cells with Latrunculin A (LatA), which blocks actin polymerization (Kueh et al., 2008). LatA treatment abrogated Ca^{2+} flux in T cells during continuous contact with anti-CD3–coated cantilevers (Fig. 3, A and D). Furthermore, both pushing

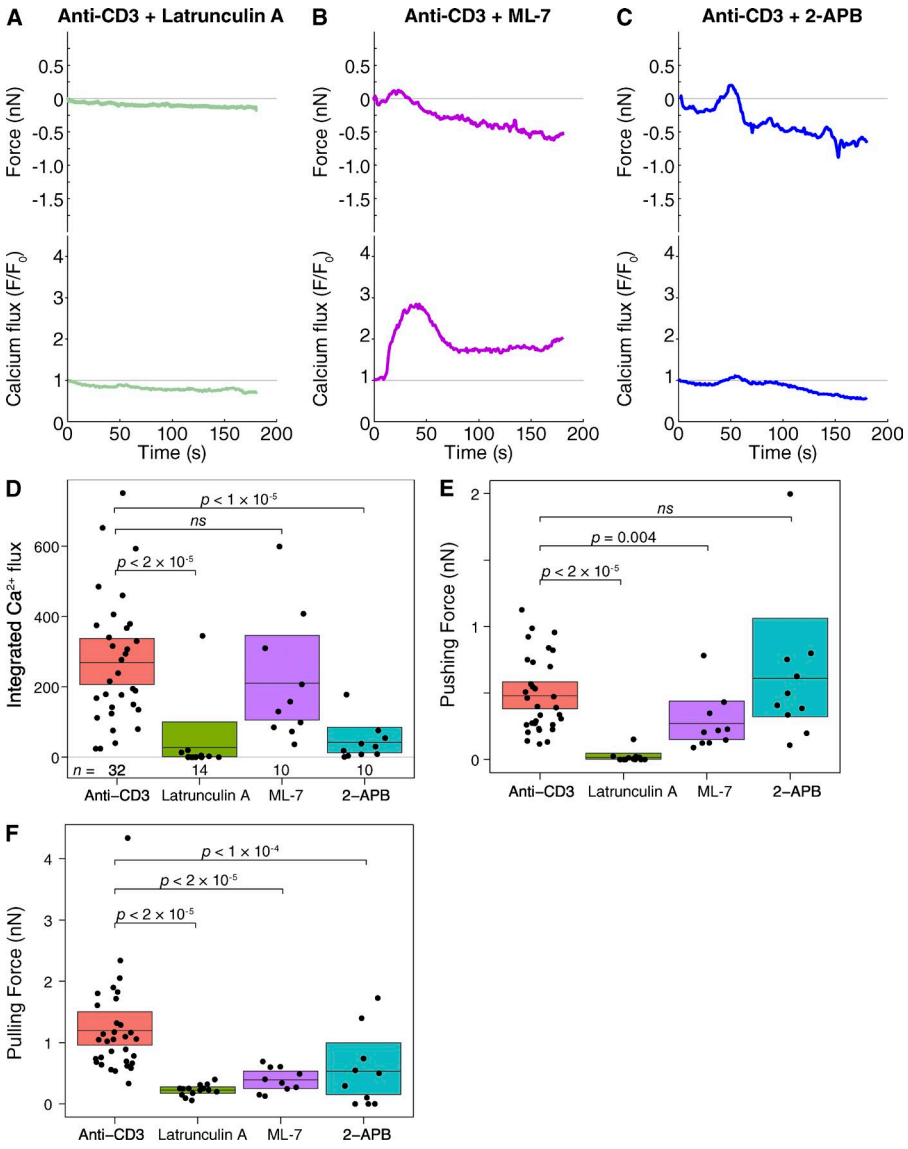

Figure 3. **Inhibitor treatments weaken force generation and Ca^{2+} flux through several mechanisms.** Time courses of both force on the cantilever and normalized Fluo-4 intensity. The AFM cantilever was brought into continuous contact with Fluo-4–labeled T cells for 180 s and imaged every 1 s. Flux was normalized to the Fluo-4 intensity at $t = 0$, when the AFM force trigger was reached upon initial contact. Cells were treated with 1 µM LatA (A), 10 µM ML-7 (B), and 40 µM 2-APB (C). Data were pooled for LatA ($n = 14$ cells from four independent experiments), ML-7 ($n = 10$ cells from two independent experiments), and 2-APB ($n = 10$ cells from two independent experiments). Comparison of integrated calcium flux (D), pushing forces (E), and pulling forces (F) for cells with or without inhibitor treatment. The pooled anti-CD3 results are the same points as in Fig 2. ns, not significant.

(Fig. 3 E) and pulling (Fig. 3 F) forces were absent. These results show that TCR ligation is not sufficient to activate T cells when the actin cytoskeleton is disabled, consistent with published findings (Varma et al., 2006).

In many systems, myosin contractility in conjunction with actin dynamics mediates traction forces. Myosin contractility plays a crucial role in T cell activation by controlling the movement of signaling microclusters at the immune synapse (Ilani et al., 2009; Yi et al., 2012). Myosin IIA activity in T cells is accelerated upon phosphorylation by myosin light chain kinase (MLCK). We tested for the role of myosin in force generation by treating with the MLCK inhibitor ML-7. We observed a significantly diminished pull force upon treatment with ML-7 compared with vehicle-treated cells (Fig. 3, B and F). The mean push force was also decreased, although to a lesser extent (Fig. 3 E). We did not observe differences in the integrated Ca^{2+} flux with ML-7 (Fig. 3 D). These results suggest that myosin IIA contractility is important in mediating force generation in T cells during activation, especially during the pull phase.

To investigate whether Ca^{2+} flux regulates the generation of force by T cells, we treated cells with 2-APB, a small-molecule blocker of the calcium release–activated channel (CRAC) (Prakriya and Lewis, 2001; Peinelt et al., 2008). We observed dramatically decreased integrated Ca^{2+} flux upon treatment (Fig. 3 C), consistent with blockade of Ca^{2+} entry through CRACs. We observed a significant decrease in the magnitude of the pulling force of 2-APB–treated cells versus controls, but pushing forces were no different (Fig. 3, E and F). This result suggests that pulling requires a sustained, elevated Ca^{2+} response. We noted, however, that there was a lack of correlation between integrated Ca^{2+} flux and pulling force (Fig. 2 F). This discrepancy could be reconciled if there were a low threshold of Ca^{2+} sufficient for achieving a maximal pulling force. We tested this notion by gathering the forces of cells stimulated with anti-CD3–coated cantilevers in the presence of 2-APB and EGTA, both of which had low Ca^{2+} flux by blocking entry of extracellular Ca^{2+}, as well as vehicle-treated cells, which had a broad range of Ca^{2+} fluxes. Indeed, we found in fitting the aggregation of these touches that pulling forces were near maximal once the integrated Ca^{2+} flux was ~200 (Fig. S2 C).

One explanation for Ca^{2+}-mediated regulation of pulling forces is that Ca^{2+}-dependent calmodulin signaling leads to MLCK activation and, subsequently, pulling forces. Indeed, loss of calmodulin leads to unresponsiveness in T cells (Lin

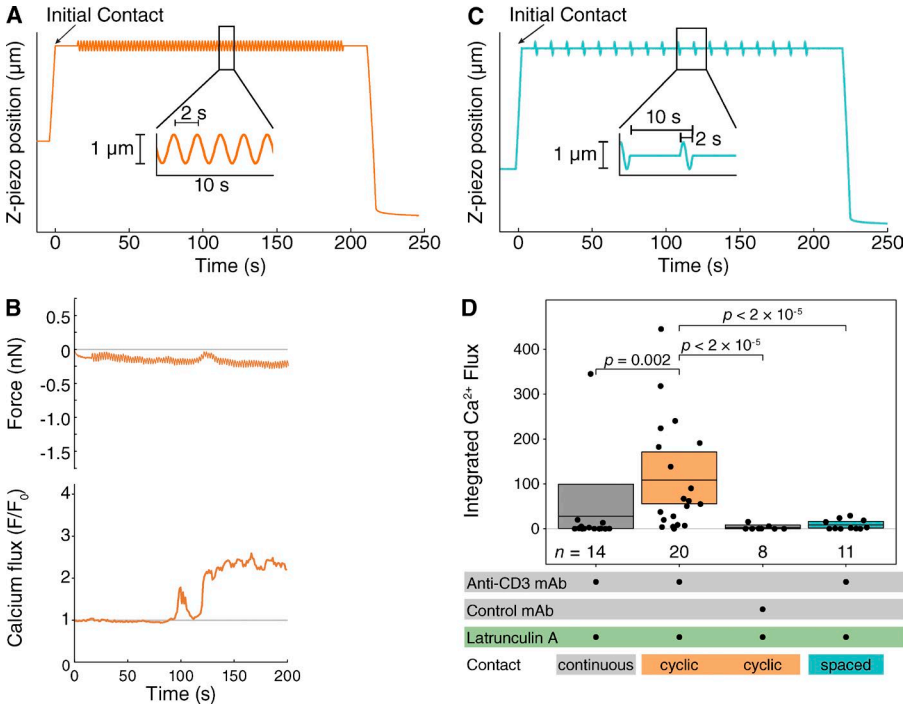

Figure 4. **Application of cyclical force rescues Ca^{2+} flux in LatA-treated cells.** (A) *Z*-position of cantilever during application of cyclical force. The ramp-up indicates lowering of the cantilever until the contact. The cantilever is held in place for 15 s and then begins a sinusoidal movement with amplitude 0.5 µm and period 2 s. After 180 s, the tip is again held constant for 15 s, then retracted. (B) Time courses for force on the cantilever and normalized Fluo-4 intensity for a cell treated with LatA subjected to the cyclical force in A. (C) *Z*-position of cantilever during the spaced cyclic force. Sinusoidal pulses from A were spaced out with constant dwells lasting 8 s, resulting in a waveform with a 10-s period. (D) Time-integrated calcium flux for LatA-treated cells with no external force, continuous cyclical force, with a spaced cyclical force or cyclical force with an irrelevant antibody. Data were pooled for LatA continuous contact (same points as Fig. 3 D), LatA cyclic contact (n = 20 cells from five independent experiments), LatA cyclic contact with control antibody (n = 8 cells from two independent experiments), and spaced cyclic contacts (n = 11 from two independent experiments). Box shows the mean and 95% CI.

et al., 2005). Our experiments perturbing Ca^{2+} entry showed that at low Ca^{2+} levels, the magnitude of the pull force became more dependent on integrated Ca^{2+} concentration. The etiology of this Ca^{2+} threshold is as yet unknown, and could be caused by calmodulin.

Numerous lines of evidence suggest that T cells "sum up" responses through sequential engagements with antigen on APCs (Faroudi et al., 2003; Henrickson et al., 2008). TCR signaling that was abbreviated induced anergy caused by nuclear factor of activated T cells (NFAT)-driven transcription (Marangoni et al., 2013). Cyclic adhesion of single-molecule pMHCs to T cells using a biomembrane force probe showed that 5-s intervals between contacts were sufficient to produce Ca^{2+} flux, whereas 10 s was insufficient (Pryshchep et al., 2014). To test whether the application of force could rescue signaling in T cells where the actin cytoskeleton was inhibited with LatA, we programmed the piezo *z*-stage of the AFM to gently engage the T cell with an anti-CD3–coated cantilever, hold position as before for 15 s, then oscillate in a sinusoidal fashion with an amplitude of 500 nm and period of 2 s (Fig. 4 A), akin to the size of invadopodia (Ueda et al., 2011). This sinusoidal movement of the cantilever translated into an ∼180 pN range of forces felt by the cell (Fig. 4 B), on par with the pushing force generated by the T cell itself (Fig. 2 C). We found to our surprise that the sinusoidal force engendered Ca^{2+} flux in LatA-treated cells (Fig. 4 B). The integrated Ca^{2+} flux for cells treated with LatA receiving an oscillatory force was significantly higher than those engaged continuously (Fig. 4 D). To determine whether oscillating force alone was driving Ca^{2+} flux, we applied the oscillating force to LatA-treated T cells, but this time using cantilevers coated with either of two control antibodies (hCD25 and CD43; Fig. S3, A and B). These conditions generated negligible Ca^{2+} flux (Fig. 4 D). Thus, cyclical force alone was insufficient to induce Ca^{2+} influx. Rather, only with concurrent engagement of TCR–CD3 was Ca^{2+} flux elicited.

We were curious whether the cyclic application of force could also strengthen signaling in the absence of LatA. We coated cantilevers with pMHC and applied either continuous or cyclical contact. Application of cyclical forces (Fig. S3 A) did not significantly increase Ca^{2+} flux compared with continuous contact (Fig. S3 B) when F-actin was intact. Thus, cyclical contact delivers equivalent antigenic signals as continuous contact when the actin cytoskeleton is unperturbed.

We next examined the frequencies (i.e., intervals between forceful pulses) that best promoted Ca^{2+} flux. We tested an intermittent signal, where single sinusoidal waves were separated by 8 s of no movement (Fig. 4 C). Contact of LatA-treated T cells with infrequent cycles did not engender Ca^{2+} flux (Fig. 4 D). This finding suggests the existence of a resetting mechanism that acts within a 10-s timescale, such that infrequent signals are insufficient for activating the T cell.

We next sought to understand the mechanism for rescue of Ca^{2+} flux in the T cell upon application of cyclical forces to the TCR. As one possible explanation, we questioned whether application of oscillatory forces to the T cell led to an increased number of TCR–CD3 engagements, thus amplifying the amount of signal the cell received. To determine whether the tip was steadily engaging more receptors, we measured the force amplitude: the adhesive forces as the cantilever retracted from the cell's surface (the upward movement of each oscillation) compared with the forces as the cantilever pushed into the surface. Increased engagement of cell receptors over time should result in larger force amplitudes, because the tip would experience increased adhesion forces as the cantilever pulled upwards. Indeed, we saw a significant increase in amplitude when we tested cyclical force in the absence of LatA (Fig. 5, B and C; and Fig. S3 A). Likely, with an intact actin cytoskeleton, the T cell pushed against the oscillating cantilever and formed more contacts with molecules on the tip over time.

In contrast, when we examined the force amplitude in the presence of LatA, we saw little to no rise in the amplitude over time (Fig. 5, A and C). The same was true for cantilevers coated with control mAbs (Fig. S3, C–F; and Fig. 5 C). From these results, we conclude that LatA treatment precluded an

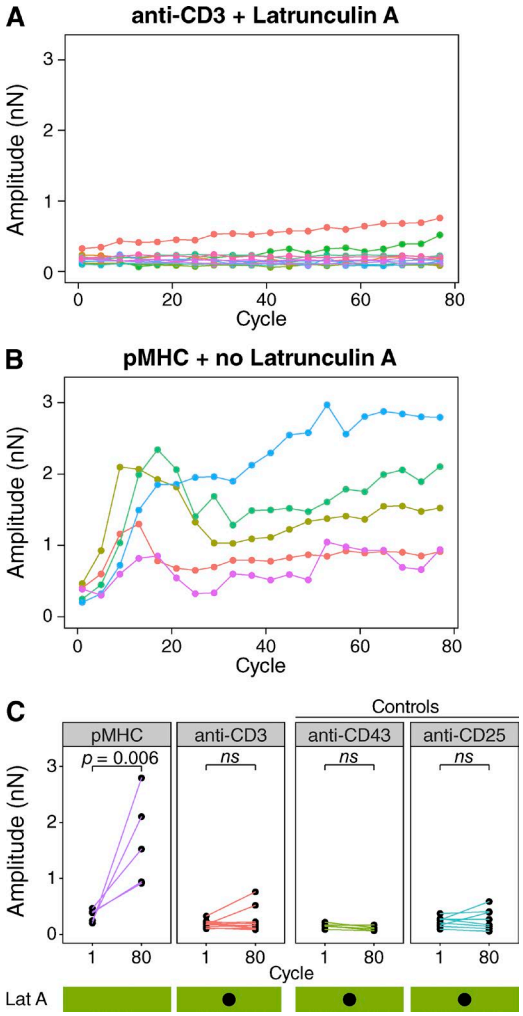

Figure 5. **Cyclical force in LatA-treated cells does not increase the number of engagements.** Amplitude of force oscillations over time during application of cyclical forces for LatA-treated cells with anti-CD3–treated (A) and control-treated (B) cells with pMHC-coated tips. For clarity, every fourth cycle is plotted, showing amplitude from maxima to minima. (C) Comparison of force amplitudes for the first cycle (1) and the final cycle (80), showing that treatment with LatA blocks an increase in force oscillations over the experiment. Data were pooled for cyclic contacts with pMHC without LatA (n = 5 cells from two independent experiments), cyclic contacts with anti-CD3 with LatA (same cells as Fig. 4), cyclic contacts with anti-CD43 (n = 5 cells), and cyclic contacts with anti-hCD25 (same cells as Fig. 4). ns, not significant.

increase in the number of engaged receptors. We therefore posit that cyclic mechanical forces act by increasing the signal per engaged receptor rather than the number of engaged receptors when F-actin is inhibited.

In addition to this work, others have shown that application of external mechanical force on the TCR through anti-CD3 antibodies or pMHC is capable of inducing Ca^{2+} entry (Kim et al., 2009a; Li et al., 2010). One proposed mechanism for mechanosensation by the TCR is a conformational change model, wherein mechanical forces are transduced through the TCR–CD3 complex (Kim et al., 2009b), resulting in exposure of buried ITAM motifs (Xu et al., 2008; Das et al., 2015). Oscillating forces delivered exogenously or generated at the lamellipodium (Sims et al., 2007) could be required to unbury these ITAM-bearing domains.

In conclusion, our findings suggest a mechanical–chemical positive feedback loop, whereby initial TCR engagements result in local force generation by the T cell through cytoskeletal rearrangement. These forces enable spreading and rhythmic oscillation of the lamellipodium and act to both increase the number of contacts and enhance signaling from existing ones. Cyclical forces applied to T cells that cannot generate their own forces rescue this process. We showed that application of cyclical force alone with control antibodies elicited negligible Ca^{2+} responses. Thus, pure mechanical stimulation is not sufficient; rather, the mechanical forces must be delivered through engagement of the TCR. We hypothesize that some short-lived signaling intermediate is formed during force-associated TCR triggering, and the life of that intermediate is less than 10 s, not unlike the same interval observed in previous work (Pryshchep et al., 2014). The identity of this time-dependent signaling pathway is unknown, though our AFM-based approach will be useful for dissecting the role of candidate pathways.

Materials and methods

Mice, cell lines, and reagents

All primary murine $CD4^+$ T cells came from homozygous OT-II TCR transgenic mice (Taconic). The following antibodies were used in this study: biotinylated anti–human-CD25 (clone BC96), biotinylated anti-CD3ε (clone 145-2C11), biotinylated anti-CD43 (clone 1B11), and anti-CD28 (clone 37.51) from BioLegend, and anti-CD3ε (clone 145-2C11) from Bio X Cell. Biotinylated I-A^b presenting OVA(323–339) was obtained from the National Institutes of Health Tetramer Facility for pMHC studies. Ovalbumin peptide 323–339 was obtained from AnaSpec, and recombinant human interleukin-2 was obtained from Prometheus. Latrunculin A was obtained from Cayman Chemical, ML-7 from Santa Cruz Biotechnology, Inc., and 2-APB from Abcam.

Preparation of primary murine $CD4^+$ T cells

T cells from OT-II mice were isolated from spleen and lymph nodes using $CD4^+$ EasySep immunomagnetic separation (STEMCELL Technologies). Cells were activated on plate-bound anti-CD3ε (8 µg/ml) with 2 µg/ml anti-CD28 for 2 d before being taken off and maintained in interleukin-2–containing medium. Cells were assayed 4 d after activation.

Fluorescence imaging

All fluorescence images were collected on a Nikon Ti-E system fitted with a 40× Plan Fluor objective, NA 0.6. Excitation of fluorophores was done using epifluorescence excitation from a halogen lamp light source (Sutter Instrument). The Chroma 49002-ET-EGFP (FITC/Cy2) filter cube was used for excitation and emission of Fluo-4. For pseudoratiometric imaging, cells were loaded with 3.75 µM Fura-Red concurrently with 1 µM Fluo-4 at 25°C for 45 min. Cells were washed twice before use. To image Fluo-4 and Fura-Red intensity simultaneously, we excited the cells using epifluorescence excitation through a 470/40 filter. Emitted light was passed through a Photometrics DV2 Dualview with 525/40 and 630/50 dichroics. The mean intensity of Fluo-4 signal was divided by mean intensity of Fura-Red signal to get the ratio shown. Images were collected using an intensified CCD camera (XR/MEGA-10; Stanford Photonics). Image acquisition was controlled using µManager (https://micro-manager.org). Custom code written with MATLAB (MathWorks) using the Image Processing Toolbox was used to identify cell areas for the calcium studies.

Atomic force microscopy

AFM was conducted using an Asylum Research MFP 3D-BIO system combined with a Nikon inverted microscope (Ti-E). The cantilevers used were HYDRA6R-200N (AppNano). Cantilevers were mounted before touching the cell, and inverse optical lever sensitivities and spring constants were calibrated on a bare glass surface. Cells were loaded with appropriate dyes and then allowed to settle on poly-D-lysine–coated 50-mm Fluorodishes (World Precision Instruments). Cells were kept in imaging media (phenol red–free RPMI plus 5% FBS, Hepes, and penicillin/streptomycin). The dish was maintained at 37°C using the Asylum Research Petri heater. In the experiments described, the cantilever was lowered onto cells with the tip positioned approximately at the middle of the cell area. The cantilever tip was gently lowered toward the cell at a speed of 2 µm/s until the specified force trigger was achieved. The cantilever remained in contact with the cell either unmoving or programmed to execute rhythmic piezo-*z* movements. Finally, the cantilever was fully retracted. We collected Fluo-4 fluorescence images at 1 frame/s and AFM deflection data at 20,000 Hz. To synchronize acquisition of data from the AFM and microscope, we used custom LabView code and a PCI-6115 board (National Instruments) to acquire the analog deflection and piezo-*z* channels from the AFM controller, digital pulses from the AFM controller corresponding to the start and trigger point of each touch, and digital pulses from µManager (Edelstein et al., 2014) via a DT9816 board (Data Translation) corresponding to frames of the camera. These data were processed and analyzed using custom code written in MATLAB.

Chemical conjugation of AFM cantilevers

HYDRA6R-200N tips were plasma-cleaned and bathed in acetone with 4% (3-mercaptopropyl)-trimethoxysilane (Sigma-Aldrich). After 2 h, tips were removed; washed with acetone, isopropanol, and water; and cured for 1 h at 110°C under vacuum.

Streptavidin (Jackson ImmunoResearch Laboratories, Inc.) was reacted with sulfo-LC-SPDP using free amine groups on streptavidin and the sulfo-NHS ester in PBS plus 1 mM EDTA, pH 7.5. The reaction mix was passed through a Zeba Desalt column (89882; Thermo Fisher Scientific) to remove unreacted cross-linker. The resulting product was then reacted with the free sulfhydryl groups on the silanized cantilevers overnight at 4°C. Streptavidin-bonded tips were washed in PBS, bathed in a solution of 25 µg/ml biotinylated antibody (anti-CD3, anti-hCD25, or anti-CD43), and washed again in PBS. For the pMHC-coated tips, streptavidin-bonded cantilevers were bathed in a solution of biotinylated I-A^b-OVA(323–339) at 50 µg/ml.

Statistical analyses

Fluorescence data were scaled to the intensity at the trigger point. Time-integrated fluorescence intensity was calculated using a trapezoidal approximation. Deflection data were decimated down to 20 Hz. Force data were obtained from the deflection in volts by multiplying by inverse optical lever sensitivity and spring constant. The maximum push force was calculated for the largest peak after trigger time. The push force had as its baseline the nearest prior inflection point as determined by custom code in MATLAB, not necessarily the 0-force baseline. Maximum pull force was calculated from the 0-force baseline to the absolute minimum force in the time series.

Permutation testing was used for all statistical comparisons of calcium flux and force generation. Permutation is superior to the classic *t* test as it does not require a normally distributed population. We used the permutationTest2 function of the Resample package of R (Hesterberg, 2015) to calculate p-values and determine 95% CIs, performing 100,000 permutations. All error boxes in all figures show the bootstrapped mean and 95% CI.

Online supplemental material

Fig. S1 shows the cross-linking strategy, the chemical strategy of covalently attaching streptavidin to the cantilever using a sulfo-LC-SPDP cross-linker. Fig. S2 shows pseudoratiometric imaging of calcium influx, showing that Fluo-4 intensity rise is caused by Ca^{2+} concentration increase, not shape change of the cell. Fig. S3 shows that application of cyclic force in the absence of LatA does not significantly increase signaling strength compared with continuous contact. Online supplemental material is available at http://www.jcb.org/cgi/content/full/jcb.201511053/DC1.

Acknowledgments

We thank Dr. T. Thauland for critical feedback on the manuscript and Dr. M.A. Bruce for software.

Financial support came from the National Institutes of Health/National Institute of General Medicine Sciences (R01 GM110482 to M.J. Butte and T32 GM008294 to K.H. Hu), the Stanford Children's Health Research Institute, the Morgridge Family Foundation, and the National Science Foundation (CBET 1264833 to M.J. Butte).

The authors declare no competing financial interests.

Submitted: 14 November 2015
Accepted: 10 May 2016

References

Beemiller, P., and M.F. Krummel. 2010. Mediation of T-cell activation by actin meshworks. *Cold Spring Harb. Perspect. Biol.* 2:a002444. http://dx.doi.org/10.1101/cshperspect.a002444

Billadeau, D.D., J.C. Nolz, and T.S. Gomez. 2007. Regulation of T-cell activation by the cytoskeleton. *Nat. Rev. Immunol.* 7:131–143. http://dx.doi.org/10.1038/nri2021

Bunnell, S.C., D.I. Hong, J.R. Kardon, T. Yamazaki, C.J. McGlade, V.A. Barr, and L.E. Samelson. 2002. T cell receptor ligation induces the formation of dynamically regulated signaling assemblies. *J. Cell Biol.* 158:1263–1275. http://dx.doi.org/10.1083/jcb.200203043

Das, D.K., Y. Feng, R.J. Mallis, X. Li, D.B. Keskin, R.E. Hussey, S.K. Brady, J.H. Wang, G. Wagner, E.L. Reinherz, and M.J. Lang. 2015. Force-dependent transition in the T-cell receptor β-subunit allosterically regulates peptide discrimination and pMHC bond lifetime. *Proc. Natl. Acad. Sci. USA.* 112:1517–1522. http://dx.doi.org/10.1073/pnas.1424829112

Edelstein, A.D., M.A. Tsuchida, N. Amodaj, H. Pinkard, R.D. Vale, and N. Stuurman. 2014. Advanced methods of microscope control using µManager software. *J. Biol. Methods.* 1:1. http://dx.doi.org/10.14440/jbm.2014.36

Faroudi, M., R. Zaru, P. Paulet, S. Müller, and S. Valitutti. 2003. Cutting edge: T lymphocyte activation by repeated immunological synapse formation and intermittent signaling. *J. Immunol.* 171:1128–1132. http://dx.doi.org/10.4049/jimmunol.171.3.1128

Henrickson, S.E., T.R. Mempel, I.B. Mazo, B. Liu, M.N. Artyomov, H. Zheng, A. Peixoto, M.P. Flynn, B. Senman, T. Junt, et al. 2008. T cell sensing of antigen dose governs interactive behavior with dendritic cells and sets a threshold for T cell activation. *Nat. Immunol.* 9:282–291. http://dx.doi.org/10.1038/ni1559

Hesterberg, T. 2015. Resampling Functions. R package version 0.4. https://cran.r-project.org/web/packages/resample/index.htm (accessed May 12, 2016).

Hosseini, B.H., I. Louban, D. Djandji, G.H. Wabnitz, J. Deeg, N. Bulbuc, Y. Samstag, M. Gunzer, J.P. Spatz, and G.J. Hämmerling. 2009. Immune synapse formation determines interaction forces between T cells and antigen-presenting cells measured by atomic force microscopy. *Proc. Natl. Acad. Sci. USA.* 106:17852–17857. http://dx.doi.org/10.1073/pnas.0905384106

Hu, K.K., M.A. Bruce, and M.J. Butte. 2014. Spatiotemporally and mechanically controlled triggering of mast cells using atomic force microscopy. *Immunol. Res.* 58:211–217. http://dx.doi.org/10.1007/s12026-014-8510-7

Ilani, T., G. Vasiliver-Shamis, S. Vardhana, A. Bretscher, and M.L. Dustin. 2009. T cell antigen receptor signaling and immunological synapse stability require myosin IIA. *Nat. Immunol.* 10:531–539. http://dx.doi.org/10.1038/ni.1723

James, J.R., and R.D. Vale. 2012. Biophysical mechanism of T-cell receptor triggering in a reconstituted system. *Nature.* 487:64–69. http://dx.doi.org/10.1038/nature11220

Kim, D.H., P.K. Wong, J. Park, A. Levchenko, and Y. Sun. 2009a. Microengineered platforms for cell mechanobiology. *Annu. Rev. Biomed. Eng.* 11:203–233. http://dx.doi.org/10.1146/annurev-bioeng-061008-124915

Kim, S.T., K. Takeuchi, Z.Y. Sun, M. Touma, C.E. Castro, A. Fahmy, M.J. Lang, G. Wagner, and E.L. Reinherz. 2009b. The alphabeta T cell receptor is an anisotropic mechanosensor. *J. Biol. Chem.* 284:31028–31037. http://dx.doi.org/10.1074/jbc.M109.052712

Kueh, H.Y., G.T. Charras, T.J. Mitchison, and W.M. Brieher. 2008. Actin disassembly by cofilin, coronin, and Aip1 occurs in bursts and is inhibited by barbed-end cappers. *J. Cell Biol.* 182:341–353. http://dx.doi.org/10.1083/jcb.200801027

Lee, S.J., Y. Hori, and A.K. Chakraborty. 2003. Low T cell receptor expression and thermal fluctuations contribute to formation of dynamic multifocal synapses in thymocytes. *Proc. Natl. Acad. Sci. USA.* 100:4383–4388. http://dx.doi.org/10.1073/pnas.0630563100

Li, Y.C., B.M. Chen, P.C. Wu, T.L. Cheng, L.S. Kao, M.H. Tao, A. Lieber, and S.R. Roffler. 2010. Cutting Edge: mechanical forces acting on T cells immobilized via the TCR complex can trigger TCR signaling. *J. Immunol.* 184:5959–5963. http://dx.doi.org/10.4049/jimmunol.0900775

Lin, M.Y., T. Zal, I.L. Ch'en, N.R. Gascoigne, and S.M. Hedrick. 2005. A pivotal role for the multifunctional calcium/calmodulin-dependent protein kinase II in T cells: From activation to unresponsiveness. *J. Immunol.* 174:5583–5592. http://dx.doi.org/10.4049/jimmunol.174.9.5583

Liu, B., W. Chen, B.D. Evavold, and C. Zhu. 2014. Accumulation of dynamic catch bonds between TCR and agonist peptide-MHC triggers T cell signaling. *Cell.* 157:357–368. http://dx.doi.org/10.1016/j.cell.2014.02.053

Ma, Z., and T.H. Finkel. 2010. T cell receptor triggering by force. *Trends Immunol.* 31:1–6. http://dx.doi.org/10.1016/j.it.2009.09.008

Malissen, B., and P. Bongrand. 2015. Early T cell activation: Integrating biochemical, structural, and biophysical cues. *Annu. Rev. Immunol.* 33:539–561. http://dx.doi.org/10.1146/annurev-immunol-032414-112158

Marangoni, F., T.T. Murooka, T. Manzo, E.Y. Kim, E. Carrizosa, N.M. Elpek, and T.R. Mempel. 2013. The transcription factor NFAT exhibits signal memory during serial T cell interactions with antigen-presenting cells. *Immunity.* 38:237–249. http://dx.doi.org/10.1016/j.immuni.2012.09.012

Negulescu, P.A., T.B. Krasieva, A. Khan, H.H. Kerschbaum, and M.D. Cahalan. 1996. Polarity of T cell shape, motility, and sensitivity to antigen. *Immunity.* 4:421–430. http://dx.doi.org/10.1016/S1074-7613(00)80409-4

Peinelt, C., A. Lis, A. Beck, A. Fleig, and R. Penner. 2008. 2-Aminoethoxydiphenyl borate directly facilitates and indirectly inhibits STIM1-dependent gating of CRAC channels. *J. Physiol.* 586:3061–3073. http://dx.doi.org/10.1113/jphysiol.2008.151365

Prakriya, M., and R.S. Lewis. 2001. Potentiation and inhibition of Ca(2+) release-activated Ca(2+) channels by 2-aminoethyldiphenyl borate (2-APB) occurs independently of IP(3) receptors. *J. Physiol.* 536:3–19. http://dx.doi.org/10.1111/j.1469-7793.2001.t01-1-00003.x

Pryshchep, S., V.I. Zarnitsyna, J. Hong, B.D. Evavold, and C. Zhu. 2014. Accumulation of serial forces on TCR and CD8 frequently applied by agonist antigenic peptides embedded in MHC molecules triggers calcium in T cells. *J. Immunol.* 193:68–76. http://dx.doi.org/10.4049/jimmunol.1303436

Puech, P.-H., D. Nevoltris, P. Robert, L. Limozin, C. Boyer, and P. Bongrand. 2011. Force measurements of TCR/pMHC recognition at T cell surface. *PLoS One.* 6:e22344. http://dx.doi.org/10.1371/journal.pone.0022344

Ritter, A.T., Y. Asano, J.C. Stinchcombe, N.M. Dieckmann, B.C. Chen, C. Gawden-Bone, S. van Engelenburg, W. Legant, L. Gao, M.W. Davidson, et al. 2015. Actin depletion initiates events leading to granule secretion at the immunological synapse. *Immunity.* 42:864–876. http://dx.doi.org/10.1016/j.immuni.2015.04.013

Sage, P.T., L.M. Varghese, R. Martinelli, T.E. Sciuto, M. Kamei, A.M. Dvorak, T.A. Springer, A.H. Sharpe, and C.V. Carman. 2012. Antigen recognition is facilitated by invadosome-like protrusions formed by memory/effector T cells. *J. Immunol.* 188:3686–3699. http://dx.doi.org/10.4049/jimmunol.1102594

Sims, T.N., T.J. Soos, H.S. Xenias, B. Dubin-Thaler, J.M. Hofman, J.C. Waite, T.O. Cameron, V.K. Thomas, R. Varma, C.H. Wiggins, et al. 2007. Opposing effects of PKCtheta and WASp on symmetry breaking and relocation of the immunological synapse. *Cell.* 129:773–785. http://dx.doi.org/10.1016/j.cell.2007.03.037

Ueda, H., M.K. Morphew, J.R. McIntosh, and M.M. Davis. 2011. CD4+ T-cell synapses involve multiple distinct stages. *Proc. Natl. Acad. Sci. USA.* 108:17099–17104. http://dx.doi.org/10.1073/pnas.1113703108

Varma, R., G. Campi, T. Yokosuka, T. Saito, and M.L. Dustin. 2006. T cell receptor-proximal signals are sustained in peripheral microclusters and terminated in the central supramolecular activation cluster. *Immunity.* 25:117–127. http://dx.doi.org/10.1016/j.immuni.2006.04.010

Xu, C., E. Gagnon, M.E. Call, J.R. Schnell, C.D. Schwieters, C.V. Carman, J.J. Chou, and K.W. Wucherpfennig. 2008. Regulation of T cell receptor activation by dynamic membrane binding of the CD3epsilon cytoplasmic tyrosine-based motif. *Cell.* 135:702–713. http://dx.doi.org/10.1016/j.cell.2008.09.044

Yi, J., X.S. Wu, T. Crites, and J.A. Hammer III. 2012. Actin retrograde flow and actomyosin II arc contraction drive receptor cluster dynamics at the immunological synapse in Jurkat T cells. *Mol. Biol. Cell.* 23:834–852. http://dx.doi.org/10.1091/mbc.E11-08-0731